Dynamic behavior of a spring-powered micronozzle needle-free injector

Published Version:
Dynamic behavior of a spring-powered micronozzle needle-free injector / Schoubben A.; Cavicchi A.; Barberini L.; Faraon A.; Berti M.; Ricci M.; Blasi P.; Postrioti L.. - In: INTERNATIONAL JOURNAL OF PHARMACEUTICS. - ISSN 0378-5173. - ELETTRONICO. - 491:1-2(2015), pp. 91-98. [10.1016/j.ijpharm.2015.05.067]

Availability:
This version is available at: https://hdl.handle.net/11585/703579 since: 2020-02-25

Published:
DOI: http://doi.org/10.1016/j.ijpharm.2015.05.067

*Graphical Abstract (for review)

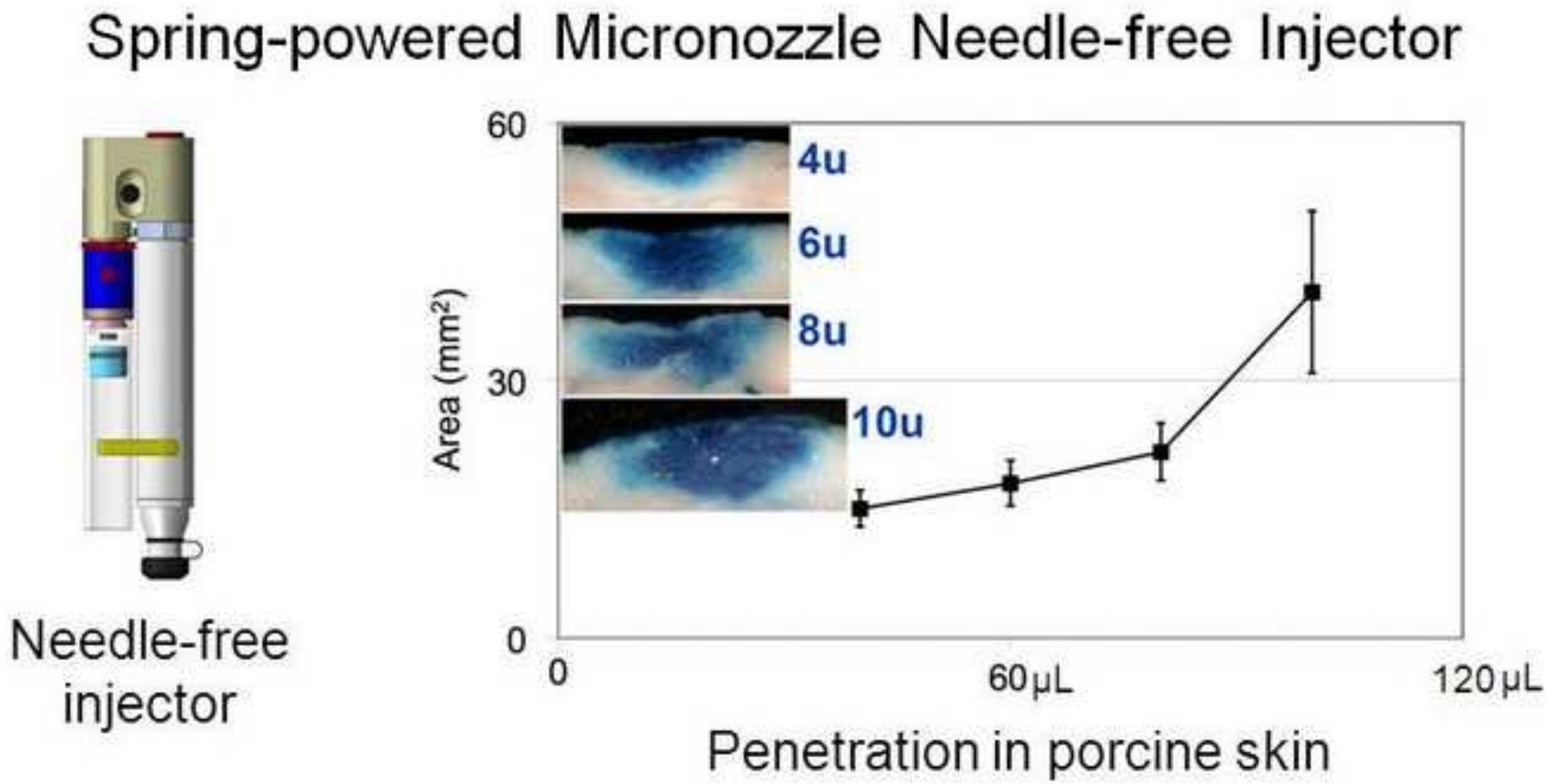

DYNAMIC BEHAVIOR OF A SPRING-POWERED MICRONOZZLE NEEDLE-FREE INJECTOR

Aurélie Schoubben[1], Andrea Cavicchi[2], Lanfranco Barberini[3], Alessio Faraon[4], Marco Berti[4], Maurizio Ricci[1], Paolo Blasi[5*], Lucio Postrioti[2*]

[1] Dipartimento di Scienze Farmaceutiche, Università degli Studi di Perugia, Perugia, Italy

[2] Dipartimento di Ingegneria, Università degli Studi di Perugia, Perugia, Italy

[3] Dipartimento di Chimica, Biologia e Biotecnologie, Università degli Studi di Perugia, Perugia, Italy

[4] Brovedani Group, San Vito al Tagliamento, Italy

[5] School of Pharmacy, University of Camerino, Via Sant'Agostino 1, 62032, Camerino, Italy.

* Corresponding Authors:

Paolo BLASI, e-mail: paolo.blasi@unicam.it; phone +39 0737402289, fax: +39 0737637345.

Lucio POSTRIOTI, e-mail: lucio.postrioti@unipg.it; Phone/fax: +39 0755853733

Abstract

Conventional injection is still the leading method to deliver macromolecular therapeutics. Needle injection is considered a low compliance administration strategy, principally due to pain and needle phobia. This has fostered the research on the development of alternative strategies to circumvent the skin barrier. Among needle-free drug delivery methods, jet injection is an old strategy with great potential not yet completely disclosed. Here, the design, engineering and dynamic behavior of a novel spring-powered micronozzle needle-free injector is presented. Fluid mechanics was first studied in air to calculate jet force and speed as well as injection duration in different conditions. Polyacrylamide gel was used to simulate a soft tissue and to investigate the jet evolution over time of different injected doses. Finally, *ex vivo* characterization was carried out on pig skin. Results evidenced a direct dependence of the force, velocity, and duration with the injection volume. The model material allowed individuating the different steps of jet penetration and to attempt a mechanistic explanation. A different behavior has been recorded in the skin with interesting findings for subcutaneous and/or dermal delivery. Peculiar features with respect to existing jet injectors confers to this device good potentiality for a future clinical application.

Keywords: spring-powered needle-free injectors, jet injectors, micronozzle, transdermal delivery, and insulin.

List of symbols and abbreviations

API, active pharmaceutical ingredient;

v, speed at the nozzle exit section;

m, injected mass;

Δt, injection duration;

ρ, density of the solution

A, nozzle outflow section;

F, force;

p, pressure;

Δy, distance between the nozzle and the target;

$\Delta t_{(n \rightarrow t)}$, time of flight from nozzle to target;

L_t, penetration depth in pig skin (mm);

L_m, distance from the skin surface and the maximum width;

Q, volumetric flow rate;

μ, dynamic viscosity;

L, needle length;

D, needle bore diameter;

As, syringe stopper area;

C_d, discharge coefficient.

1. Introduction

Conventional injection, syringe provided with needle, is at the moment the leading method to deliver macromolecular therapeutics. Transdermal drug delivery offers a number of advantages, especially when biological macromolecules are the therapeutics to be delivered (Prausnitz and Langer 2008). Needle injection is considered a low compliance administration strategy, particularly when applied to chronic therapies. Pain during administration and needle phobia are the factors limiting its compliance. This has fostered the research on the development of new strategies for transdermal delivery: these include formulation strategies and devices able to circumvent the skin barrier avoiding conventional needles.

Formulation strategies comprise the addition of penetration enhancer (i.e., additives able to reduce the skin barrier proprieties) (Williams and Barry 2004) or the inclusion of the active pharmaceutical ingredient (API) in a carrier able to cross the skin (Cevc 2004). Pro-drug approach has been also found useful but API chemical modification is not always feasible (Puglia et al. 2006).

Devices capable to puncture the skin and deliver therapeutics without the use of a conventional needle (e.g., needle-free injectors, micro needles) are a reliable alternative to conventional injections (Arora et al. 2007; van der Maaden et al. 2012; Xiang et al. 2013). Needle-free jet injectors have been conceived to minimize pain and inconvenience in parenteral therapy. Invented more than a century ago, liquid jet injectors were firstly used in clinics for mass immunization only in the 1950's (Mitragotri 2012).

The basic components of a liquid jet injector are a compressed gas or a spring, a piston, a compartment where the formulation is loaded, and a nozzle. These devices use the gas or the spring as power source to push the piston that impress a pressure to the liquid formulation that, as a reaction, is ejected through the nozzle orifice at high velocity ($v > 100$ m/s). Nozzle orifices have been produced with diameters ranging from 76 to 360 µm but the most used devices had orifice diameter of about 150 µm (Mitragotri 2013). The liquid jet pierces the *stratum corneum* delivering the established formulation volume subcutaneously. From the engineering point of view, they are easy to produce and relatively cheap because neither electrical power nor electronic parts are required. From the clinical side, they are easy to handle, are applicable virtually to all liquid formulations and may improve their pharmacokinetics (Schramm and Mitragotri 2002).

Paradoxically, one of the drawbacks that seems to limit the large clinical use of needle-free jet injectors seems to be the pain but this issue is still controversial (Schneider et al. 1994; Zsigmond

2002). More critical are the inconsistency of formulation penetration and the pool out of liquid on the skin (Mitragotri 2012). The latter limits intra- and inter-individual reproducibility of the key pharmacokinetics parameters with obvious issues on formulation bioequivalence. This inconsistency seems to be device related because some of them have shown even better pharmacokinetic and pharmacodynamic parameters than conventional injection (Engwerda et al. 2011; Engwerda et al. 2013).

Most of the mentioned drawbacks are due to the limited number of systematic studies on the key parameters involved in jet formation, skin penetration and drug delivery to tissue as well as the lack of studies aimed at crossing these parameters with clinical data.

One possible solution to the pain generated by the jet could be the use of smaller orifice (i.e., 80 µm) to generate a high-velocity microjet ($v > 100$ m/s). This solution has been proposed and validated for the delivery of nanoliter volumes (Arora et al. 2007). Here we propose a novel device provided with a micronozzle for medium volume skin delivery that could cover the gap between microjets and conventional jet injectors.

The design (Figure 1) and the full characterization of the dynamic behavior of a novel spring-powered needle-free liquid jet injector are reported below.

2. Materials and methods

2.1. Materials

Acrylamide, bis-acrylamide, tetramethylethylenediamine and ammonium persulfate were purchased from Bio-Rad Laboratories (Segrate, Italy) while methylene blue was obtained by Sigma (Milan, Italy).

Porcine skin was kindly provided by the Centro Macellazione Carne (Ponte San Giovanni, Italy).

The needle-free injector mounted with an 80 µm nozzle was produced and provided by Brovedani spa (San Vito al Tagliamento, Italy). All other reagents and products were of the highest grade commercially available and used as received.

2.2. Dynamic performance characterization

The injector was characterized in terms of dynamic performances by loading and injecting different volumes of distilled water (40, 80 and 120 µL). Each test was repeated 5 times and the following data were recorded:

- Mass of liquid shot by the injector, computed as a difference of device weight, before and after the shot;
- Impact force on a target positioned at 17 mm from the nozzle hole. The impact force was measured with a high-sensitivity, piezoelectric force sensor (Kistler Type 9215, Kistler Holding AG, Winterthur, Switzerland). From these data it was possible to gain information about the momentum flux through the nozzle hole and the duration of the injection process.

2.2.1. Average speed measurement

The average outlet speed from the nozzle was computed knowing time duration of the shot and the mass of the volume injected as reported in the following equation;

$$\frac{m}{\Delta t} = \rho A v \rightarrow v = \frac{m}{\rho A \Delta t} \qquad \text{Equation 1}$$

where v is the speed at the nozzle exit section, m is the injected mass, Δt the injection duration, ρ the density of the solution and A the nozzle outflow section (Arora et al. 2007; Schramm and Mitragotri 2002; Schramm-Baxter and Mitragotri 2004a).

2.2.2. Impact force and instantaneous velocity measures

The nozzle outflow velocity was calculated from the force signal. The impact force on the target is equal to the momentum flux through the nozzle hole, if the following hypotheses are verified (Postrioti and Battistoni 2010; Postrioti et al. 2012):

- Steady flow;
- The jet is orthogonally deviated by the target, so to lose at the impact its velocity component directed towards the target itself.

The maximum, minimum, and mean force values as well as the corresponding speed values have been calculated using the following equation;

$$F = \rho A v^2 \rightarrow v = \sqrt{\frac{F}{\rho A}} \qquad \text{Equation 2}$$

The pressure into the nozzle can be evaluated applying Bernoulli equation upstream and downstream the nozzle hole. The maximum pressure was calculated from the force signal using the momentum equation.

$$\frac{p}{\rho} + \frac{v^2}{2} = cost. \rightarrow p = \frac{\rho v^2}{2} = \frac{F}{2A} \qquad \text{Equation 3}$$

2.2.3. Jet tip speed

The jet tip speed was estimated from the video analysis. For every acquisition two frames were extracted: the first at the beginning of the injection and the second at the impact against the target. Knowing the sequence number of the frames and the time delay between two consecutive frames (equal to 1/fps), the time spent by the jet tip to reach the target was defined. The distance covered in mm was the measure in pixel multiplied by the image scale factor. So the average jet speed is:

$$v = \frac{\Delta y}{\Delta t(n \rightarrow t)} \qquad \text{Equation 4}$$

2.3. In vitro motion studies

2.3.1. Polyacrylamide gel preparation

Polyacrylamide gel was used as a model soft material to mimic human epidermal tissue texture (Schramm-Baxter et al. 2004; Stachowiak et al. 2009). Acrylamide and bis-acrylamide were solubilized in distilled water at 4 and 0.16% (w/v), respectively. Initiators (N,N,N′,N′-tetramethylethylenediamine, 0.005% w/v; ammonium persulfate, 0.075% w/v) were added to the solution that was vigorously shaken and immediately poured in round bottom glass tubes (diameter, 12 mm; length, 55 mm; volume, 4.5 mL) and left polymerize under daylight. Complete polymerization was achieved after 1 hour.

2.3.2. Experimental setup

The analysis of the spray evolving in gel was based on a imaging system in backlight arrangement. The glass test tube containing the gel was positioned between the illumination system and the high speed camera. The set-up elements were mounted on a linear guide so to adjust their relative positions. The injector was loaded with methylene blue solution (1% w/v) to obtain a proper contrast between liquid and gel in the acquired images and the jet evolution in gel was recorded using a high speed camera (Phantom® v711, Vision Research, Wayn, NJ, USA). The high speed camera was equipped with a Nikkor 200 mm objective (Nikon), operating at high frequency (1600 frame/s) set at 60μs exposure time. The lighting system needed for this exposure time consisted of a LED matrix (48 x SMD 505, 12V) and a light diffuser. The glass tube containing the gel was placed between the LED panel and the camera. Different volumes of methylene blue solution (40, 60, 80, 100 and 120 μL), corresponding to different insulin units (4, 6, 8, 10 and 12 units), were injected and each injection was repeated 5 times.

2.3.3. Image acquisition and post-processing

Every acquisition generated a video composed of about 1000 frames acquired at a constant frame rate and covering an entire injection process. The off-line analysis of the acquired video allowed the detection of the injection process beginning that is assumed as time-zero for the following analyses. After the time-zero frame detection, selected frames were extracted from the video to quantitatively analyze the process evolution. The extracted frames time step was short at the beginning of the process, when the jet evolved quickly. Once steady flow was reached, the time step became longer. The single frame analysis was stopped at the injection process end. The first frame in which the liquid column detached from the nozzle assumed the timing of the injection end.

Each of the extracted frames was converted in a "jpg" format image and used for the quantitative analysis, by which the spray tip penetration time-history along with the jet width and area were computed by means of self-developed image analysis software written in LabVIEW Vision environment. In particular, each image was converted in a binary file setting a grey threshold level above which or under which the pixel was white for the gel or black for methylene blue. This procedure was required to convert a real-world image in grey levels to a black and white pixel image, on which it has been possible to perform geometrical measurements after color inversion to obtain a white-on-black image.

2.3.4. Measurements

The first geometrical measurement was focused on the computation of the white pixels, as an approximation of the jet volume, with the assumption of an axial-symmetric jet evolution. The jet penetration was determined defining the nozzle hole coordinates as it appeared in the sequence and moving a measuring bar starting from the opposite boundary of the image looking for the position in which the measuring bar was tangent to the jet boundary. In a conceptually similar manner, the software computed the jet width as the sum of its length in the left and right directions. The time evolution of these quantities gave important knowledge about the spray behavior in terms of tendency to correctly penetrate the gel bulk and to form a well-defined sac of the injected liquid in the gel mass.

2.4. Ex vivo characterization

Porcine skin was employed to study the depth of the penetration reached by the solution injected and the relative area developed (longitudinal section). Methylene blue solution (1% w/v) was used since it consents to easily distinguish the portion of the tissue reached by the solution injected from the rest of the tissue. Just after injection, the skin sample was frozen using a cryospray (Histofreezer®, OraSure Technologies, Inc., Bethlehem, PA, USA) and successively cut longitudinally at the injection point. The sections were photographed using stereoscope (Leica WILD M32 with WILD PLAN1X ocular) equipped with a camera (Leica DFC 320). From the photomicrographs, three different determinations were made: the measurement of the penetration depth (L_t), the distance from the skin surface corresponding to maximum width (L_m) and the estimation of the injected area (Figure 2). Different volumes of methylene blue solution (corresponding to 4, 6, 8 and 10 insulin units) were injected and the results were expressed as the mean of 10 measurements ± standard deviation.

3. Results and discussion

3.1. Needle-free injector dynamic performances

To determine the average fluid outcome velocity (Eq. 1), the injection duration was deduced from the spray impact force signal profiles (Figure 3). The actual injection duration was easily calculable since the signal start and end were well definite. The maximum and minimum forces and the duration of the injection were extracted from Figure 3 as the signal value at start and end points (Table 1). In the evaluation of the fluid outcome velocity, the initial force peak was ignored. The first force peak is actually due to the impact phenomenon onset, during which the steady flow condition cannot be considered true. Only in steady flow conditions, the impact force can be assumed as corresponding to the spray momentum flux.

The device performed a regular injection that produced a force signal with very short start and end ramps and a definite steady value in the middle. The spring pre-charge force was proportional to fluid volume to be injected. This behavior is due to the device engineering. The reservoir has a variable volume that can load from 20 to 160 μL of formulation. A revolving system in the back of the device is used to load the formulation (Figure 1). At each revolution the piston steps back increasing the volume of the loading chamber of 20 μL and the spring is compressed correspondingly. As a consequence, the tested needle-free device is characterized by an increase of the spring compression with the loading (injection volume). This implies a rise of the spray velocity and momentum flux with the injected volume. This trend was clearly confirmed by the experimental spray impact force profiles, which evidenced not only an increase of the injection process duration with the injected volume (Figure 3) but also of the impact force intensity (Table 1).

The speed values calculated using equations 1 and 2 gave similar values with a difference lower than 10%, underlining the robustness of the methods employed (Table 2).

As expected, the speed evaluated using the video analysis was lower (Table 2) since the jet tip penetration is a phenomenon mostly controlled by drag effects exerted by the gel on the injected liquid column. All values showed an increase of the speed with the increase of the volume injected. In comparison with other devices reported in literature (Stachowiak et al. 2009), the device presented here produced a faster jet.

The pressure into the nozzle increased with the increase of the volume loaded (Table 2). This is the consequence of the spring pre-charge force increase that is directly proportional to the volume loaded into the system. Maximum pressure values are generally higher than the reported for other needle-free injectors (Schramm and Mitragotri 2002). Obviously, differences can be found in the different power source and nozzle diameter; both responsible for the generation of different pressures.

Interestingly, device performances should not change significantly by increasing formulation viscosity (Fry 2014). Highly viscous liquid pharmaceutical formulations are generally difficult to handle with conventional syringes because of syringeability and injectability issues (Cilurzo et al. 2011). The large availability of high molecular weight therapeutic proteins produced with the recombinant DNA technology has renewed the interest for needle-free injectors. Large macromolecules at the desired dose may produce highly viscous solutions difficult to deliver with conventional strategies. In the viscosity range of interest, needle-free injector performances are mainly unaffected (Cilurzo et al. 2011).

In a conventional syringe provided with needle, the force necessary to extrude the formulation is proportional to its viscosity as shown in the Hagen-Poiseuille equation;

$$F = \frac{128\, Q\, \mu\, L\, As}{\pi\, D^4} \qquad \text{Equation 5}$$

where F is the syringe stopper force, Q the volumetric flow rate, μ the dynamic viscosity, L the needle length, D the needle bore diameter and As the syringe stopper area.

The force needed to extrude a liquid formulation from a needle-free device may be calculated rearranging the Bernoulli equation as follow;

$$F = 2\, \rho\, As \left(\frac{4\, Q}{C_d\, \pi\, D^2}\right)^2 \qquad \text{Equation 6}$$

where ρ is the fluid density and C_d the discharge coefficient.

The sole explicit fluid property in the equation (Eq. 6) is ρ that generally is very close to 1. To be honest, fluid viscosity is hidden in C_d but, in the range of viscosities of pharmaceutical interest, its contribution may be considered negligible.

3.2. In vitro motion data

To perform a high-speed video analysis, the key condition is that the medium used needs to be completely transparent to detect the injected fluid with an acceptable contrast. Therefore, the great advantage of using gel is its transparency to the visible light.

Sample sequences show that the jet initially goes straight into the gel in less than 1 ms and then accumulates forming a sphere or sac in the gel bulk that grows progressively (Figure 4).

The depth of linear penetration did not change much with the increase of the volume injected indicating an initial loss of momentum flux by the jet (first 10 mm). Figure 5 shows the profiles of areas evolved, that are intended just as an approximation of the injected volumes since the images analyzed were two-dimensional. This approximation is conceivable due to the anisotropic character of a randomly cross-linked gel.

The measured jet area rises linearly up to its maximum value that was reached after an increasing time-lapse with the increasing dose injected. With 4 units, the maximum area (~ 30 mm^2) was reached after about 30 ms, while it was attained after about 120 ms (~ 80 mm^2) for the highest dose (Figure 5a). From the results, it is also possible to conclude that the duration of the injection event increases linearly with the increase of the volume injected. The jet penetration computation is probably one of the most important features to characterize the spray evolution. The penetration curves rose very fast during the first milliseconds of the injection; then the increase became very slow. The injector gave similar results in terms of penetration (8-10 mm) for all the volumes injected (only data for 80 µL are shown) but the highest dose (120 µL) where a small increase of the penetration depth was observed (~ 14 mm) (Figure 5b).

In the first laps of the injection (until 20-30 ms), the injector had a wide development in the analyzed direction, possibly due to its relatively limited penetration (Figure 6). The jet development was regular and methylene blue accumulates in a sort of regular sphere that grew up progressively. This regular behavior seems to be due to the small nozzle diameter (80 µm) combined with the high actuation pressure which together cause the jet to act as a thin needle, easily penetrating in the first stratum of the gel, preserving here its shape but quickly losing its momentum later on. As shown in Figure 6, the right side and the left side of the sphere evolved in the same mode.

A mechanistic explanation of jet penetration in polyacrylamide gel has been attempted [13]. During the first 2 ms after actuation, 3 different phases have been individuated: erosion (~ 0.2 ms) followed by about 0.8 ms of stagnation and diffusion that last until the complete delivery (Schramm-Baxter et al. 2004). Differently from previous reported data (Schramm-Baxter and Mitragotri 2004; Schramm-Baxter et al. 2004; Stachowiak et al 2009), the third phase, called diffusion, generated a sphere with an additional structure growing up at later time points, leading to a jellyfish-like geometrical form (Figure 4). This behavior could be due to a combination of the gel elastic properties and the size of the tube. During diffusion the sphere grows reaching a size of the same order of magnitude of the glass tube diameter. Being a forced diffusion, it can be speculated that the equatorial elasticity of the gel decrease while approaching the glass, generating a turbulent back-flow escaping the sphere in its upper part. Differences in poly (acrylamide) gel elasticity have been recorded individuating a position-dependent (distance from the bottom) elastic modulus (Durmaz and Okay 2011). Polyacrylamide films seem to have elasticity correlated with the film thickness: thinner is the film lower is the elastic modulus (Buxboim et al. 2010).

3.3. Ex vivo characterization

Figure 7a shows that the area of the solution injected in porcine skin linearly increases from 15 to 22 mm^2 injecting the equivalent of 40, 60, and 80 µL of methylene blue (1% w/v) aqueous solution. Similarly to what observed with the measurement of the penetration depth (Figure 7b), the injection of 100 µL produced the highest area (40 mm^2) breaking the linear increase observed with the first 3 doses injected. The reproducibility was high if considering the possible variability that can be obtained working with biological tissues. This behavior correlates with what was observed during the force determination study.

Figure 7b shows that the penetration depth linearly increases from 2.7 to 3.2 mm by injecting 40, 60, and 80 µL of methylene blue (1% w/v) aqueous solution. The injection of 100 µL produced the deepest penetration (4.4 mm) without following the linearity observed with lower dosages. This behavior is probably due to the mechanical system triggering the injection that has progressively higher strength increasing the dose charged. High reproducibility was observed for the first 3 doses injected.

L_m shows a linear increase from about 0.5 to 1.5 mm when delivering 40 to 100 µL with a nozzle of 80 µm in diameter (Figure 7c). Higher values of L_m were obtained using a device mounting 152 µm nozzle and extruding at the same velocity of the injectors under investigation (Schramm-Baxter et al. 2004). Low Lt and Lm values are interesting when a subcutaneous or a dermal deposition is the aim of the administration.

Comparing the injections in polyacrylamide (Figure 4) and in pigskin (Figure 8, insert), it can be hypothesized a different jet evolution. In pigskin, the colored solution did not form neither a sphere, nor a jellyfish geometric form (Figure 7, insert). Epidermis and dermis have well-structured extra cellular matrices with an abundance of longitudinal fibers (parallel to the skin surface). It seems that the jet momentum was lost very fast and, because of fibers orientation, lateral diffusion is easily achieved (Figure 7, insert).

4. Conclusions

A novel and simple micronozzle needle-free injector has been built and characterized. Due to the small nozzle diameter it should not cause pain during injection. The device showed efficiency and reproducibility in delivering liquid formulations subcutaneously or in the intradermal space. The jet force and velocity directly increases with the volume loaded so generating an adequate penetration and diffusion for all the injected volumes. This should guarantee a complete and rapid absorption even for high volumes.

Acknowledge

Brovedani Group provided the needle-free injector and financed the research.

References

Arora, A., Hakim, I., Baxter, J., Rathnasingham, R., Srinivasan, R., Fletcher, D.A., Mitragotri, S., 2007. Needle-free delivery of macromolecules across the skin by nanoliter-volume pulsed microjets. Proc. Natl. Acad. Sci. USA. 104 (2007) 4255-4260.

Buxboim, A., Rajagopal, K., Brown, A.E.X., Discher, D.E., 2010. How deeply cells feel: methods for thin gels. J. Phys. Condens. Matter. 22, 194116-194125.

Cevc, G., 2004. Lipid vesicles and other colloids as drug carriers on the skin. Adv. Drug Deliv. Rev. 56, 675-711.

Cilurzo, F., Selmin, F., Minghetti, P., Adami, M., Bertoni, E., Lauria, S., Montanari, L., 2011. Injectability evaluation: an open issue. AAPS PharmSciTech 12, Article No. 2.

Durmaz, S., Okay, O., 2011. Inhomogeneities in poly(acrylamide) gels: position-dependent elastic modulus measurements. Polym. Bull. 46, 409-418.

Engwerda, E.E.C., Abbink, E.J., Tack, C.J., de Galan, B.E., 2011. Improved pharmacokinetic and pharmacodynamic profile of rapid-acting insulin using needle-free jet injection technology. Diabetes Care 34, 1804-1808.

Engwerda, E.E.C., Tack, C.J., de Galan, B.E., 2013. Needle-Free Jet Injection of Rapid-Acting Insulin Improves Early Postprandial Glucose Control in Patients With Diabetes. Diabetes Care 36, 3436-3441.

Fry, A., Injecting highly viscous drugs. 2014. Pharm. Tech. Europe 26, 30-32.

Mitragotri, S., Devices for overcoming biological barriers: the use of physical force, 2013. Adv. Drug Deliv. Rev. 65, 100-103.

Mitragotri, S., Mechanical disruption of skin barrier for vaccine delivery, 2012. Drug Deliv. Sys. 27, 202-212.

Postrioti, L., Battistoni, M., 2010. Evaluation of diesel spray momentum flux in transient flow conditions. SAE Technical Paper 2010-01-2244.

Postrioti, L., Mariani, F., Battistoni, M., 2012. Experimental and numerical momentum flux evaluation of high pressure diesel spray. Fuel 98, 149-163.

Prausnitz, M.R., Langer, R., 2008. Transdermal drug delivery. Nat. Biotechnol. 26, 1261-1268.

Puglia, C., Filosa, R., Peduto, A., de Caprariis, P., Rizza, L., Bonina, F., Blasi, P., 2006. Evaluation of alternative strategies to optimize ketorolac transdermal delivery, AAPS PharmSciTech 7, Article 64.

Schneider, U., Birnbacher, R., Schober, E., 1994. Painfulness of needle and jet injection in children with diabetes mellitus. Eur. J. Pediatr. 153, 409-410.

Schramm, J., Mitragotri, S., 2002. Transdermal drug delivery by jet injectors: energetics of jet formation and penetration. Pharm. Res. 19, 1673-1679.

Schramm-Baxter, J., Katrencik, J., Mitragotri, S., 2004. Jet injection into polyacrylamide gels: investigation of jet injection mechanics. J. Biomech. 37, 1181-1188.

Schramm-Baxter, J., Mitragotri, S., 2004. Needle-free jet injections: dependence of jet penetration and dispersion in the skin on jet power. J. Control. Release 97, 527-535.

Stachowiak, J.C., Li, T.H., Arora, A., Mitragotri, S., Fletcher, D.A., 2009. Dynamic control of needle-free jet injection. J. Control. Release 135, 104-112.

van der Maaden, K., Jiskoot, W., Bouwstra, J., 2012. Microneedle technologies for (trans)dermal drug and vaccine delivery. J. Control. Release 161, 645-655.

Williams, A.C., Barry, B.W., 2004. Penetration enhancers. Adv. Drug Deliv. Rev. 56, 603-618.

Xiang, Z., Wang, H., Pant. A., Pastorin. G., Lee, C., 2013. Development of vertical SU-8 microneedles for transdermal drug delivery by double drawing lithography technology. Biomicrofluidics 7, 066501.

Zsigmond, E.K., 2002. Jet anesthesia and jet local anesthesia for the 21st century. J. Natl. Med. Assoc. 94, 1004-1006.

Table 1. Maximum and minimum force signals and injection duration obtained with different volumes.

Volume (μL)	Force (N)		Δt (s)
	Maximum	Minimum	
40	0.1318	0.1012	0.0456
80	0.1548	0.1076	0.0912
120	0.1792	0.1174	0.1344

Table(s)

Table 2. Speed and pressure data calculated using different equations.

Volume (μL)	Speed (m/s)					Maximum pressure (bar)
	Eq. 1	Eq. 2			Eq. 4	Eq. 3
		Maximum	Minimum	Mean		
40	184.8	182.1	159.5	170.8	53.97	165.7
80	190.8	197.3	164.5	180.9	59.22	194.7
120	196.2	212.3	171.8	192.1	61.93	225.3

Figure captions

Figure 1. Design of the Brovedani Nebulizer.

Figure 2. Photomicrograph of porcine skin longitudinal sections injected with methylene blue using the needle-free injector and representation of the method used to estimate methylene blue area. a) photomicrograph of porcine skin longitudinal sections injected with methylene blue using the needle-free injector and indication on how Lt and Lm were determined, b) photomicrograph transformed in black and white; c) quantification of the area of deposition (in red).

Figure 3. Impact force signal profiles obtained injecting 40, 80 and 120 μL of methylene blue (1% w/v) aqueous solution.

Figure 4. Frame sequence obtained with the needle-free injector by injecting 60 μL of methylene blue (1% w/v) aqueous solution.

Figure 5. (a) Area profiles obtained injecting 40, 60, 80, 100 and 120 μL of methylene blue (1% w/v) aqueous solution in polyacrylamide gel. **(b)** Depth of penetration profiles obtained injecting 80 and 120 μL of methylene blue (1% w/v) aqueous solution in polyacrylamide gel.

Figure 6. Left and right width profiles of the area obtained injecting 40, 60, 80, 100 and 120 μL of methylene blue (1% w/v) aqueous solution (from up to down) in polyacrylamide gel.

Figure 7. Plots of different measures done on porcine skin injected with 40, 60, 80, and 100 μL of methylene blue (1% w/v) aqueous solution. ***Insert:*** Photomicrographs of porcine skin longitudinal sections after injection 40, 60, 80, and 100 μL of methylene blue (1% w/v) aqueous solution, corresponding to 4, 6, 8 and 10 insulin units. **(a)** Area of penetration profiles; **(b)** maximum depths (L_t) reached by the injected solutions; (c) distance from the skin surface to the maximum width reached in the skin.

Figure(s)

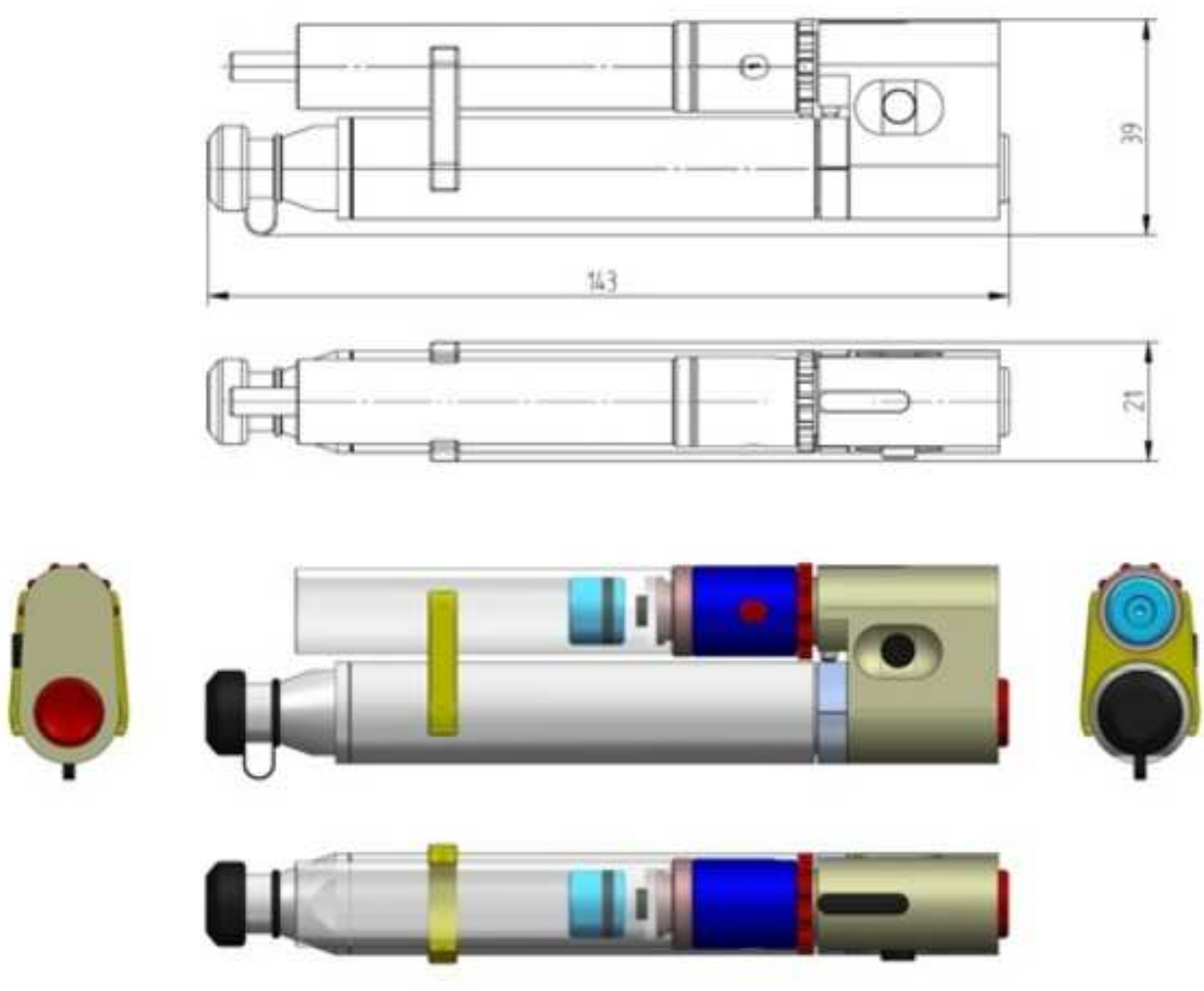

Figure(s)

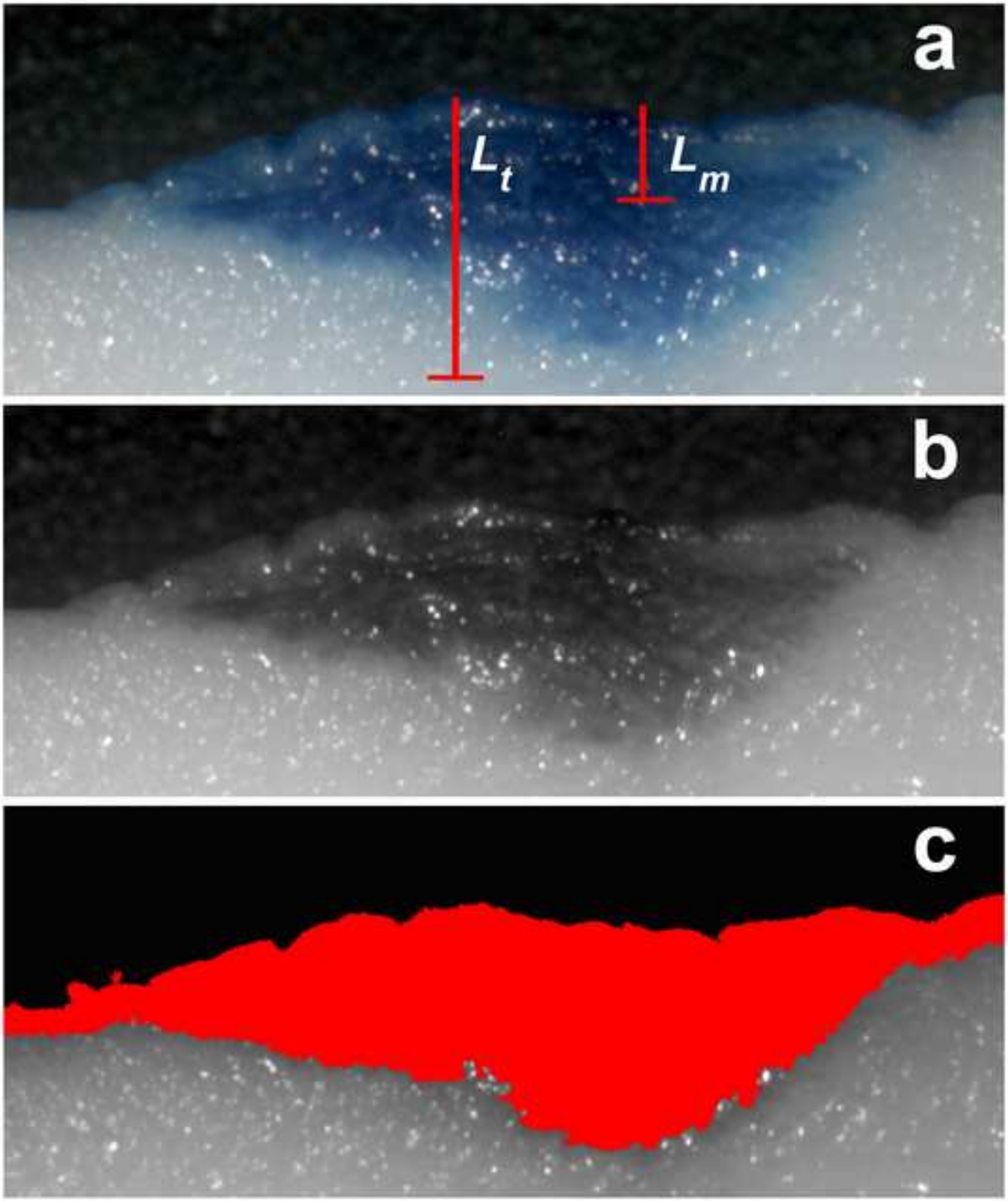

Figure(s)

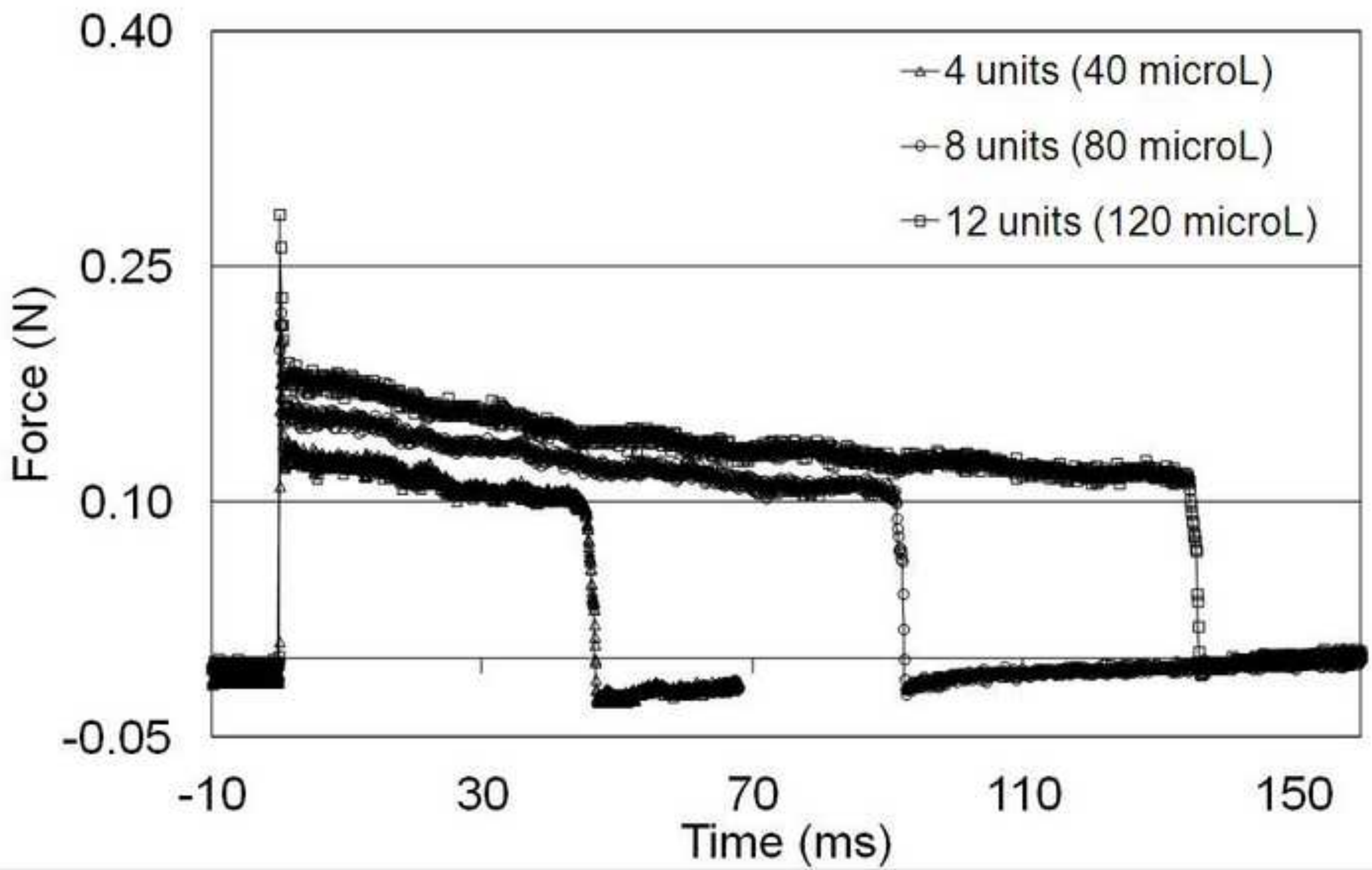

0.40
0.25
0.10
-0.05
Force (N)
-10
30
70
110
150
Time (ms)
4 units (40 microL)
8 units (80 microL)
12 units (120 microL)

Figure(s)

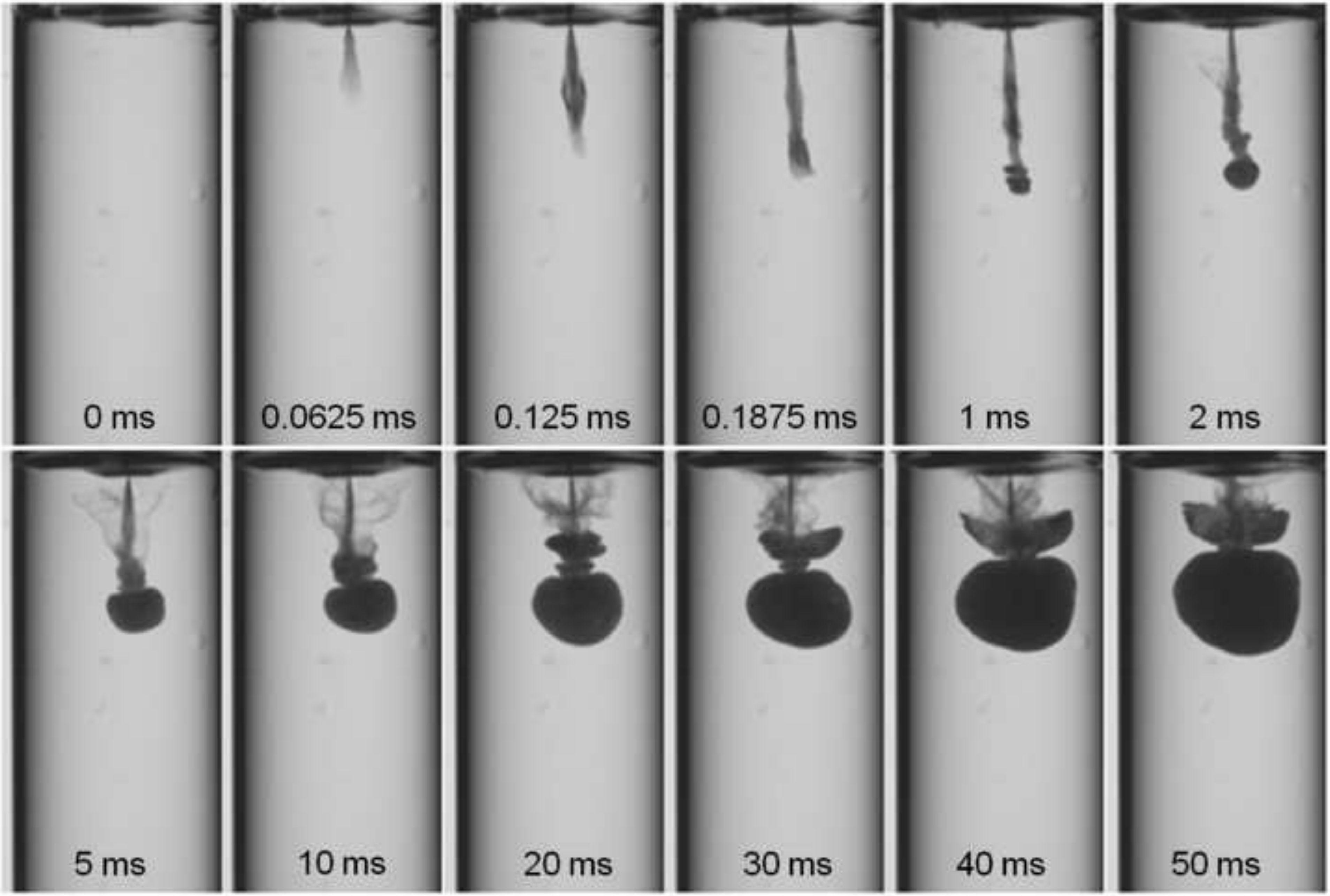
0 ms
0.0625 ms
0.125 ms
0.1875 ms
1 ms
2 ms
5 ms
10 ms
20 ms
30 ms
40 ms
50 ms

Figure(s)

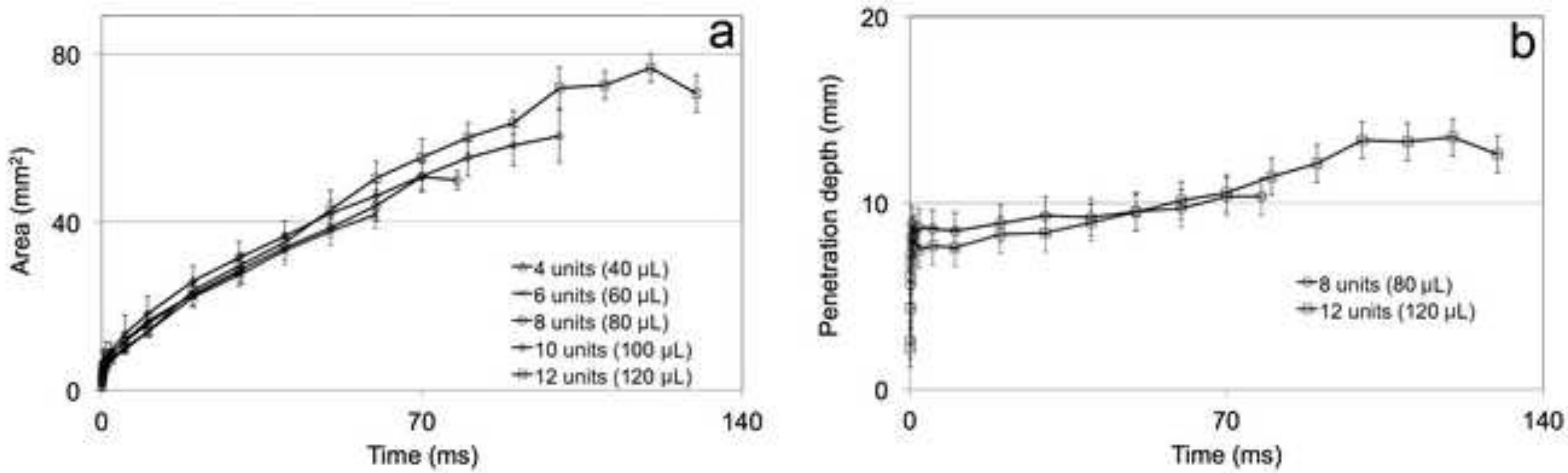
a
80
40
0
Area (mm²)
0
70
140
Time (ms)
4 units (40 µL)
6 units (60 µL)
8 units (80 µL)
10 units (100 µL)
12 units (120 µL)
b
20
10
0
Penetration depth (mm)
0
70
140
Time (ms)
8 units (80 µL)
12 units (120 µL)

Figure(s)

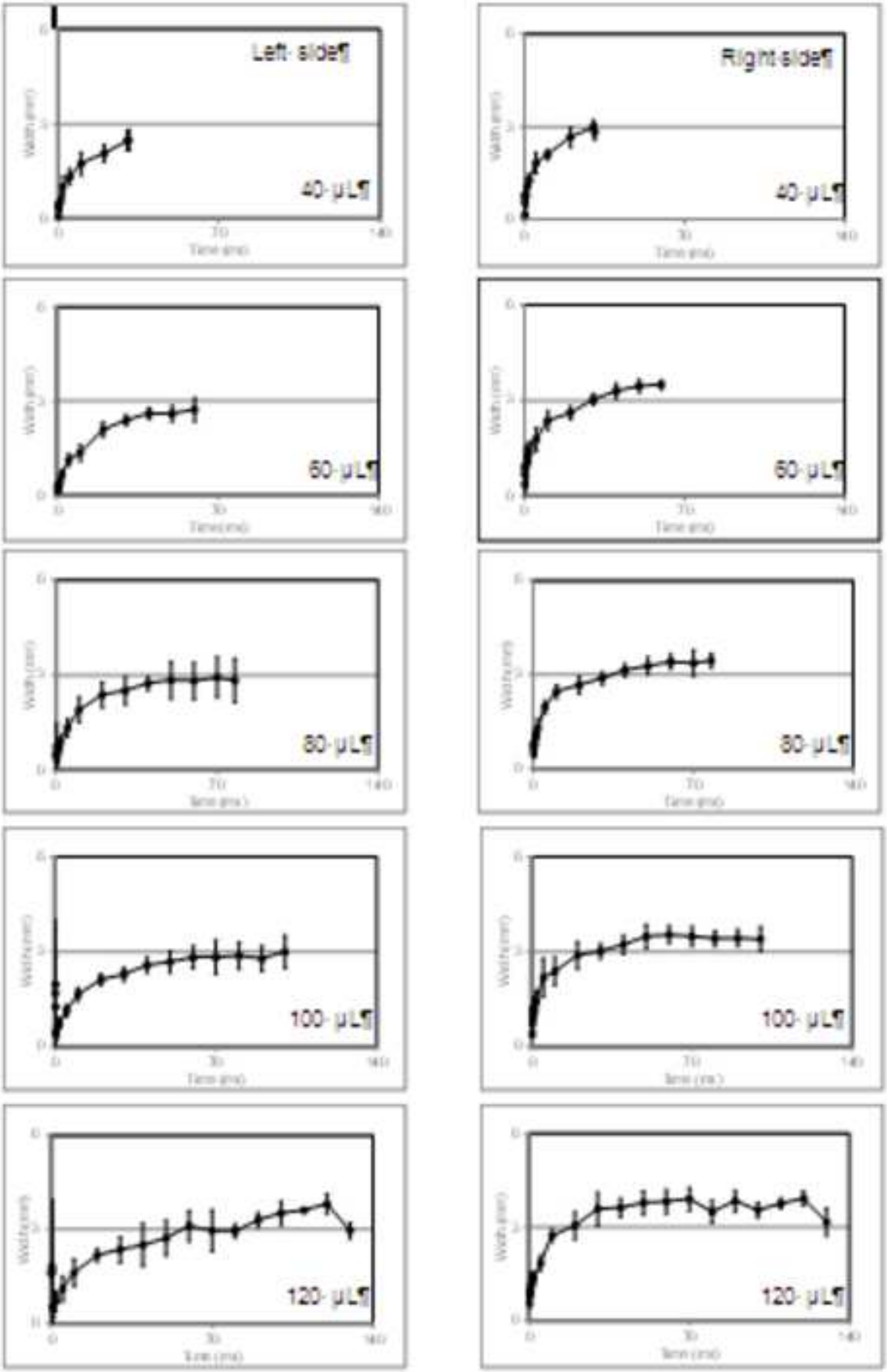
Left side¶
40 µL¶
Right side¶
40 µL¶
60 µL¶
60 µL¶
80 µL¶
80 µL¶
100 µL¶
100 µL¶
120 µL¶
120 µL¶

Figure(s)

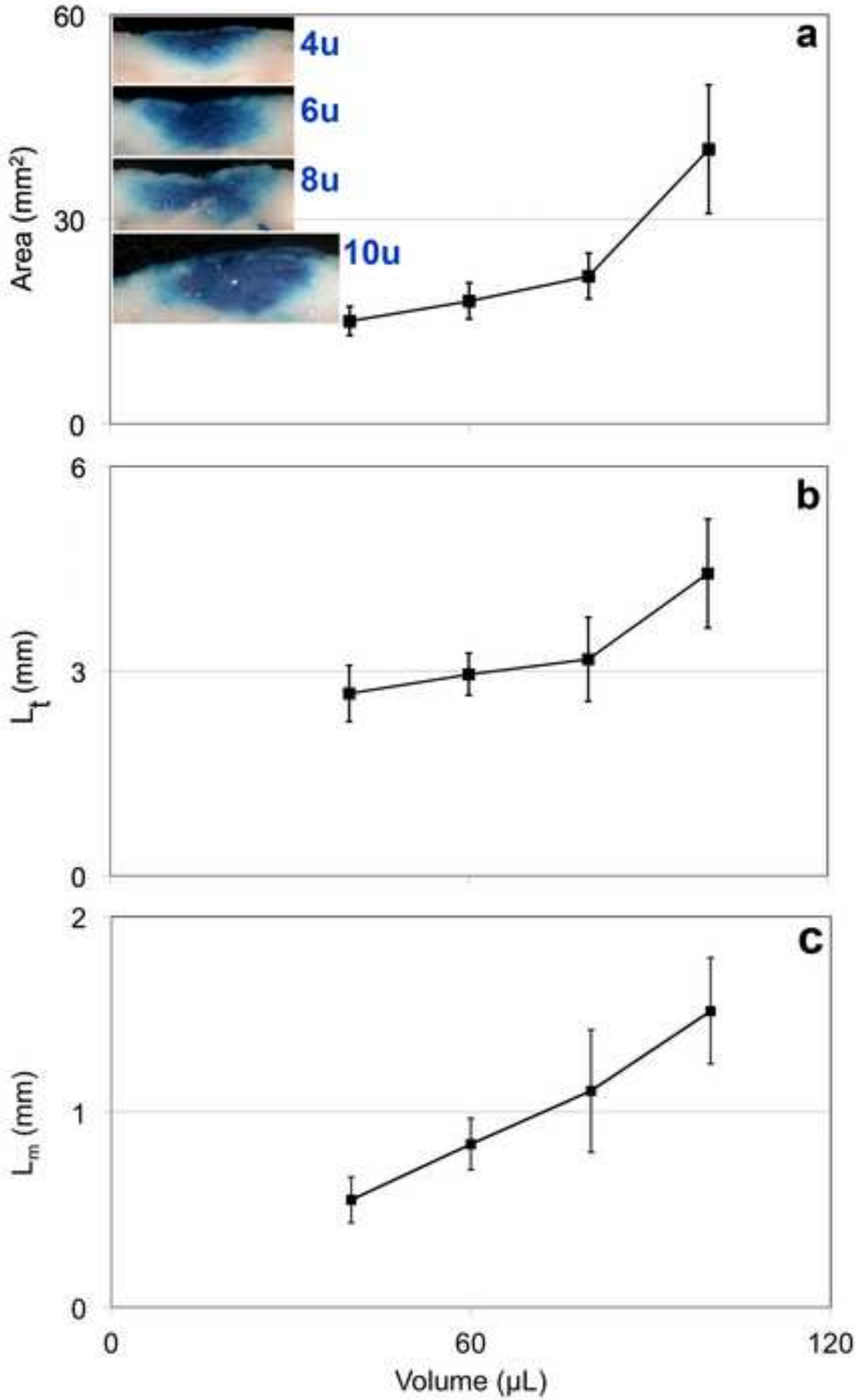

60
30
0
Area (mm²)
4u
6u
8u
10u
a
6
3
0
Lt (mm)
b
2
1
0
Lm (mm)
c
0
60
120
Volume (µL)